Thermal Gradient Infrared Spectroscopy for Diffusion in Polymers

Authors: Ashley David,^{1,2} Micah Silverman,^{1,2} Kyoungmin Kim,³ Daniel Hallinan Jr.^{1,2,*} Affiliations:

- ¹ Florida A&M University-Florida State University College of Engineering, Tallahassee, FL 32310, USA.
- ² Aero-propulsion, Mechatronics, and Energy Center, Tallahassee, FL 32310, USA.
- ³ Storagenergy Technologies, Inc., Salt Lake City, UT 84104, USA.

Keywords: FTIR-ATR, Temperature gradient, Thermal diffusion, Polymer electrolyte, LiTFSI salt, polystyrene-poly(ethylene oxide) block copolymer

Abstract

Time-resolved Fourier transform infrared-attenuated total reflectance spectroscopy (FTIR-ATR) was used to measure diffusion in opaque and translucent samples. FTIR-ATR was used to measure the change in absorbance near the heated ATR crystal surface. The infrared absorbance was then related to concentration through the Beer-Lambert law. The sample used is a polymer electrolyte composed of lithium bis-trifluoromethanesulfonylimide (LiTFSI) salt in a block copolymer polystyrene-poly(ethylene oxide) (SEO). A new approach to introduce concentration gradients is presented using a temperature gradient that creates a small salt concentration gradient due to thermally driven mass diffusion (the Soret effect). This first method was compared to a second method that we have reported using two laminated polymer electrolyte films of different salt concentrations. The thermal gradient study (Method 1) covered three temperature differences of 10°C, 15°C, and 20°C, while the second study (Method 2) used three average molar ratios, across isothermal temperatures ranging from 80°C to 120°C. The benefits and limitations of the new approach are reported, as is the activation energy for salt diffusion in this and similar SEO electrolytes. Developing new techniques to measure diffusion coefficients effectively will aid in the development of a variety of devices including solid-state batteries and thermogalvanic cells that are able to convert waste heat into electricity and improve the efficiency of power generating systems. FTIR-ATR overcomes previous limitations to experimental techniques measuring diffusion coefficients. The

^{*}Corresponding author email: dhallinan@eng.famu.fsu.edu

results prove that thermal gradient FTIR-ATR is an effective and repeatable approach for determining Fickian diffusion coefficients in viscoelastic solids.

Introduction

Analyzing transport properties in solid polymer electrolytes (SPEs) has been a topic of interest for their use in solid-state, rechargeable, lithium-metal batteries. 1-3 Currently available Li-ion batteries that use liquid electrolytes can fail catastrophically and are not compatible with next-generation, high energy density electrodes such as lithium metal. There is a need to meet the growing demands of the energy market, which is expected to double by 2050 ⁴ and is driven by an increasing number of portable electronic devices, as well as electric vehicles.^{2, 5} Solid polymer electrolytes offer low cost, safety, good flame resistance, and enable more energy dense batteries via their compatibility with lithium metal anodes.^{6, 7} Poly(ethylene oxide) (PEO) has been heavily studied as a polymer for SPEs in lithium batteries since the 1970s, when Fenton et al. found that lithium salts dissolved in PEO to form ions that can move with the polymer chain segments, providing ion conduction.^{8, 9} PEO-based electrolytes are currently the highest ionic conductivity dry polymer electrolyte and widely used as polymeric component in solid battery electrolytes.³ Block copolymers, such as high molecular weight polystyrene-poly(ethylene oxide) (SEO), are desirable for combining ion transport with high mechanical strength due to the rigid polystyrene (PS) block.^{2, 10}

For electrochemical devices that use SPEs, a successful design depends on the behavior of the current carrying species. Transport properties which describe ion transport in a binary electrolyte, such as a polymer/salt system, are ionic conductivity, salt diffusion coefficient, and cationic transference number. The most important battery metric related to transport is charge/discharge rate, which is limited by these transport properties; this highlights the importance of measuring the diffusion coefficient. Previously, self-diffusion coefficients in polymer electrolytes were studied with pulsed field gradient nuclear magnetic resonance (PFG-NMR). However, connecting self-diffusion to limiting battery rate requires the thermodynamic factor, which accounts for deviation from ideality; it must be determined through additional experiments. From the fast transverse relaxation (T2) time, which the

mobile ions in the material also have.²⁰ Another approach is restricted diffusion.^{6, 21} It infers concentration gradient from cell potential, but errors will arise from nonlinear concentration gradients caused by concentration-dependent transport and thermodynamic factors.² Therefore, Fourier Transform infrared (FTIR) spectroscopy is proposed.

FTIR can be used to find the infrared absorption, emission, and photoconductivity of solids, liquids, and gases.^{22, 23} Most often it is used to identify the presence of inorganic and organic compounds (through functional groups) in a sample from their IR 'fingerprint'. It has also been used to determine changes in concentration, e.g. for surface characterization of nanoparticles²⁴ and extraction of lipids from skin.²⁵ FTIR with attenuated total reflectance (FTIR-ATR) has been used increasingly over the past five decades as an *in-situ* technique to gain insight on diffusion in polymers from the molecular level.^{26, 27} In most prior work, diffusion of a liquid or vapor in a polymer was examined, but there have been few studies of all solid systems.²⁸ FTIR directly measures a quantity that is proportional to molar concentration, which is relevant to the mutual diffusion coefficient that plays a role in battery rate capability. Thus, FTIR overcomes limitations of the aforementioned diffusion measurement techniques. Moreover, we have developed a custom, air-free ATR set-up that is essential for battery electrolytes.^{2, 29}

As demonstrated previously, time-resolved FTIR-ATR provides a direct measurement of the salt diffusion coefficient.²⁹ In this work, we have further developed the technique in order to overcome complicated sample preparation procedures required by the need to stack two polymer electrolyte membranes of different concentration. The custom-made ATR set-up reported here allows for a temperature gradient to be rapidly applied to a sample. This results in a small concentration gradient due to the Soret effect,³⁰ as determined in our prior work,³¹ and verified here. Then, the temperature gradient can be removed, returning the system to equilibrium, and the transient response of the system can be collected. Thus, it is possible to measure the Fickian diffusion coefficient by returning to isothermal conditions and tracking the dissipation of the concentration gradient.

In this study, the Beer-Lambert Law is used to correlate FTIR absorbance and concentration. This quantification has been proven previously in all concentrations investigated of LiTFSI in PEO, in Kim et al., meaning FTIR-ATR spectroscopy can be used to measure diffusion in concentrated, all-solid systems. Concentration-based diffusion and thermal-gradient-based diffusion measurements from the multifaceted FTIR-ATR technique are reported and discussed in this paper. The results demonstrate that thermal gradient FTIR-ATR is an effective way to measure diffusion coefficients in solid PEO-based electrolytes.

Experimental

Materials

Polymer electrolyte membranes were composed of polystyrene-b-poly(ethylene oxide) (SEO) and LiTFSI. SEO synthesis and electrolyte preparation followed previously described methods.³² The weight fraction of PS, as measured with NMR, is 0.56, with the balance being PEO. The number average molecular weight of PEO is 117 kg/mol. and that of PS is 149 kg/mol. The dispersity (£) of the polymer is 1.1. Before use, SEO and LiTFSI were dried under vacuum for 48 hours at 120 °C. Then, they were moved into an argon-filled glovebox (0.1 ppm H₂O and O₂) and individually weighed on an analytical balance (Mettler Toledo, XS105, 0.01 mg resolution). The appropriate amount of LiTFSI was added to SEO to achieve a molar ratio, $r = 0, 0.05, 0.10, \text{ or } 0.15 \text{ mol}_{\text{LiTFSI}}/$ mol_{FO}. EO stands for ethylene oxide monomer repeat unit of PEO. The two solutes were then dissolved in dimethylformamide (DMF) in a 10 wt% by solids mixture. The solution was allowed to dissolve for 24 hr at 50 °C and 300 RPM. The solution was then cast onto nickel foil on a level plate and allowed to dry for 24 hours at 60°C, then under vacuum at 90 °C for 24 hours. The membranes were next folded and pressed in the glovebox using a manual hot press at 90 °C to form thicker films. Two different thicknesses were examined in this study: one film was on the order of 100 μm, and the other film had a thickness of $300 \pm 15 \,\mu m$. Thickness was measured using a micrometer (Mitituyo, 1 µm resolution). These pressed films were then punched into 3/16" diameter disks. The actual thickness of each sample was used in analyzing the data to extract each diffusion coefficient.

Temperature-gradient FTIR-ATR Spectroscopy

A heated Golden Gate ATR accessory (Specac) and custom copper anvil connected to a water-bath, were used in conjunction with the FTIR spectrometer (Frontier, PerkinElmer). The cold side temperature was controlled by the water bath, which was recirculated at high flow rate through the copper anvil. The hot side temperature was controlled by the Golden Gate ATR accessory via resistive heating. Both controllers have a resolution of 0.1°C. All FTIR measurements were taken on the hot side, at the diamond ATR crystal surface. A schematic of the setup is shown in Figure 1. The water-cooled copper anvil controls the temperature of the top of the sample. The temperature of the bottom of the sample, in contact with the ATR crystal, is controlled by the heated plate.

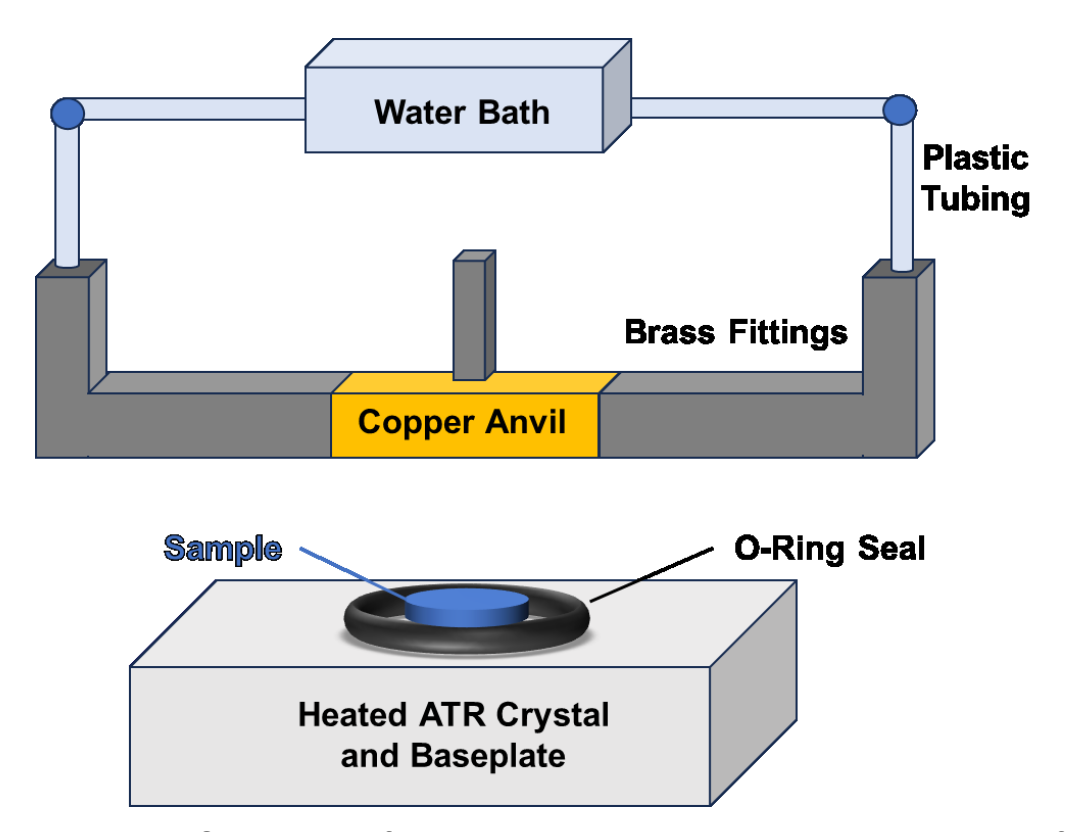


Figure 1. Schematic of FTIR-ATR setup and copper anvil design for temperature induced diffusion (Method 1), with the water bath and heated ATR baseplate creating a temperature gradient. Shown in the open position for clarity; copper anvil is lowered onto O-ring and sample to seal and press sample to ATR crystal for experiment.

To account for the significant temperature bleed occurring between the hot side, controlled by the Golden Gate, and the cold side, controlled by the water bath, a temperature calibration was conducted as described in the Supporting Information. Reported temperatures in this work are based on the temperature at the sample surface as determined by two thermocouples used during the temperature calibration.

Before placing the sample onto the FTIR, background scans were taken and saved for subtraction. These background scans were taken at each set of desired boundary temperatures: 65°C/75°C, 62.5°C/77.5°C, 60°C/80°C, as well as equilibrium: 70°C/70°C. After the background scans were taken, the anvil was disconnected from the water bath, and compressed air was used to flush water from the anvil. Next, the anvil was placed in the oven for 15 minutes at 120 °C to ensure it was dry before being cycled into the glove box.

The polymer electrolyte samples were then loaded onto the diamond ATR crystal in an argon-filled glove box. Each punched sample was placed on the ATR crystal, which was first cleaned with acetonitrile and dried using Kimwipes. The sample was sealed shut by first lowering the copper anvil down onto a sealing O-ring. Next, the anvil's torque-limited screw knob was used to press the polymer electrolyte sample to the ATR crystal with a limiting force of 40 lbs. The ATR accessory was removed from the glove box and returned to the FTIR. After loading the ATR accessory, 30 minutes were allowed for purging and thermal equilibration of the sample and the liquid nitrogen cooled, mercury cadmium telluride (MCT) detector before taking measurements.

Time-resolved FTIR spectra are the average of 8 accumulations with a fixed time interval of 10 s. The resolution is 4 cm⁻¹ from 4,000 to 450 cm⁻¹. To begin a thermal diffusion experiment, the set-points are changed from 70 °C / 70 °C to that for the desired boundary temperatures and spectra collected for 360 minutes (6 hours). As shown in Table 1, all sets of boundary temperatures were centered around 70 °C. The thermal gradients used in this work range from 0.03 °C/ μ m, for a temperature difference of 10 °C across a 300 μ m thick sample, to 0.2 °C/ μ m, for a temperature difference of 20 °C across a 100 μ m thick sample. The water bath temperature was lowered quickly from 70 °C by pouring ice into the bath. The time on the FTIR at which the temperatures reach their set point is taken as time zero, which was generally less than 8 minutes to

reach steady state. Each sample is exposed to each temperature gradient and then returned to the isothermal state with no temperature gradient (70 °C / 70 °C). Spectra are also collected for 6 hours on the return to isothermal. Thus, thermal diffusion is measured upon application of thermal gradient, and Fickian diffusion is measured upon return to isothermal state. Once all three temperature gradient trials are completed, the sample is replaced, and the process is repeated with a new sample.

Table 1. Temperatures applied, which are the actual temperatures of the 'hot' and 'cold' sides of the sample.

Water Bath	Golden Gate
T (°C)	T (°C)
65	75
62.5	77.5
60	80

The background spectra and time-resolved data from PerkinElmer's Timebase software were collected in energy units and processed in MATLAB. The background was subtracted, and intensity was converted to absorbance as $A = -log(I/I_0)$. Time zero was taken as the time at which set points were reached. The datasets were truncated to the time at which equilibrium was achieved (absorbance stopped changing). For samples of $100 \pm 5 \, \mu m$ thickness this was $5,000 \, s$, and for samples of $300 \pm 15 \, \mu m$ thickness it was $10,000 \, s$. The CF₃ peak of LiTFSI, between the wavenumbers of 1156 cm⁻¹ and 1215 cm⁻¹, was analyzed by subtracting a linear baseline and integrating the area under the peak. The CF₃ peak was chosen due to the separation from other vibrational peaks, and the pronounced change of its intensity with changing concentration. The integrated absorbance (peak area) was normalized using the following equation:

$$\frac{A(t)-A(0)}{A(\infty)-A(0)} = \frac{C_A(t)-C_A(0)}{C_A(\infty)-C_A(0)} \tag{1}$$

where A(0) is the initial absorbance and $A(\infty)$ is the final absorbance. This normalized absorbance is equal to normalized concentration due to the proportionality between absorbance and concentration. The data from return to isothermal, i.e. Fickian diffusion,

was analyzed with a numerical model to determine the LiTFSI diffusion coefficient. The finite difference solution of the transient diffusion equation,

$$\frac{\mathrm{d}C_A}{\mathrm{d}t} = D_{AB} \frac{\mathrm{d}^2_{C_A}}{\mathrm{d}z^2} \tag{2}$$

was the same as our prior work,²⁹ except with a different initial condition. The LiTFSI concentration in molarity is $C_A = C_{total}X_A$, and D_{AB} is the Fickian diffusion coefficient. Both C_{total} and D_{AB} are assumed to be constant. Due to the thick films used in this work, the time-dependent solution at z=0 was used.³³ The initial condition in this work is a linear concentration profile. This is a good assumption because of the small concentration gradient that is imposed by thermal diffusion under these conditions, as we have shown previously.³¹ The boundary conditions are no flux at the ATR crystal, z=0, and at the top of the membrane, z=L.

$$\frac{\mathrm{d}C_A}{\mathrm{d}z} = 0 \text{ at } z = 0 \text{ and at } z = L \text{ for all } t \tag{3}$$

An analytical solution can also be found,²⁷ as shown in the Supporting Information.

Concentration-gradient FTIR-ATR Spectroscopy

In this method, rather than creating the concentration gradient with a temperature gradient, diffusion was induced by vertically stacking two polymer electrolyte membranes, each with a different salt concentration. We have reported this method previously and used it to determine LiTFSI diffusion coefficients in SEO polymer films at 120 °C and varying molar ratios.² The samples were characterized by the average molar ratio of the two membranes, ranging from $r_{avg} = 0.025 - 0.125$. In addition to using this established technique to validate the temperature-gradient-based approach, these experiments have been conducted at a range of temperatures to investigate the activation energy for LiTFSI diffusion in SEO.

Following the procedures described in our prior work, 29 a 1/8" hollow punch was used to cut two samples with a molar ratio difference of 0.05 $\rm mol_{Li}/mol_{EO}$. The bottom sample was an approximate thickness of $100~\mu m$, and the top sample was at least $400~\mu m$. To obtain these thicknesses, samples were folded and pressed at $100~^{\circ} C$ between two metal plates, consistent with the thermal diffusion experimental procedure. The samples were then assembled as shown in Figure 2. The lower concentration

sample was placed on the diamond ATR element. A G-10 ring ($254 \, \mu m$ thickness, 1/8" ID, 3/8" OD) was placed around the sample, followed by a Teflon washer to keep the sample centered on the ATR crystal, and finally a bottom O-ring was placed around the washer for the purpose of maintaining the sample air-free. A second G-10 ring containing the higher concentration sample (sample side down) was then placed, centered, on top of the bottom assembly. A third G-10 ring containing a disk of Teflon was placed on top. This served to press the two samples into contact after thermal equilibration. Finally, a second o-ring was placed on top of the first, and the accessory was closed. The anvil was tightened only until both o-rings had solid contact, but not enough to create contact between the samples and induce diffusion.

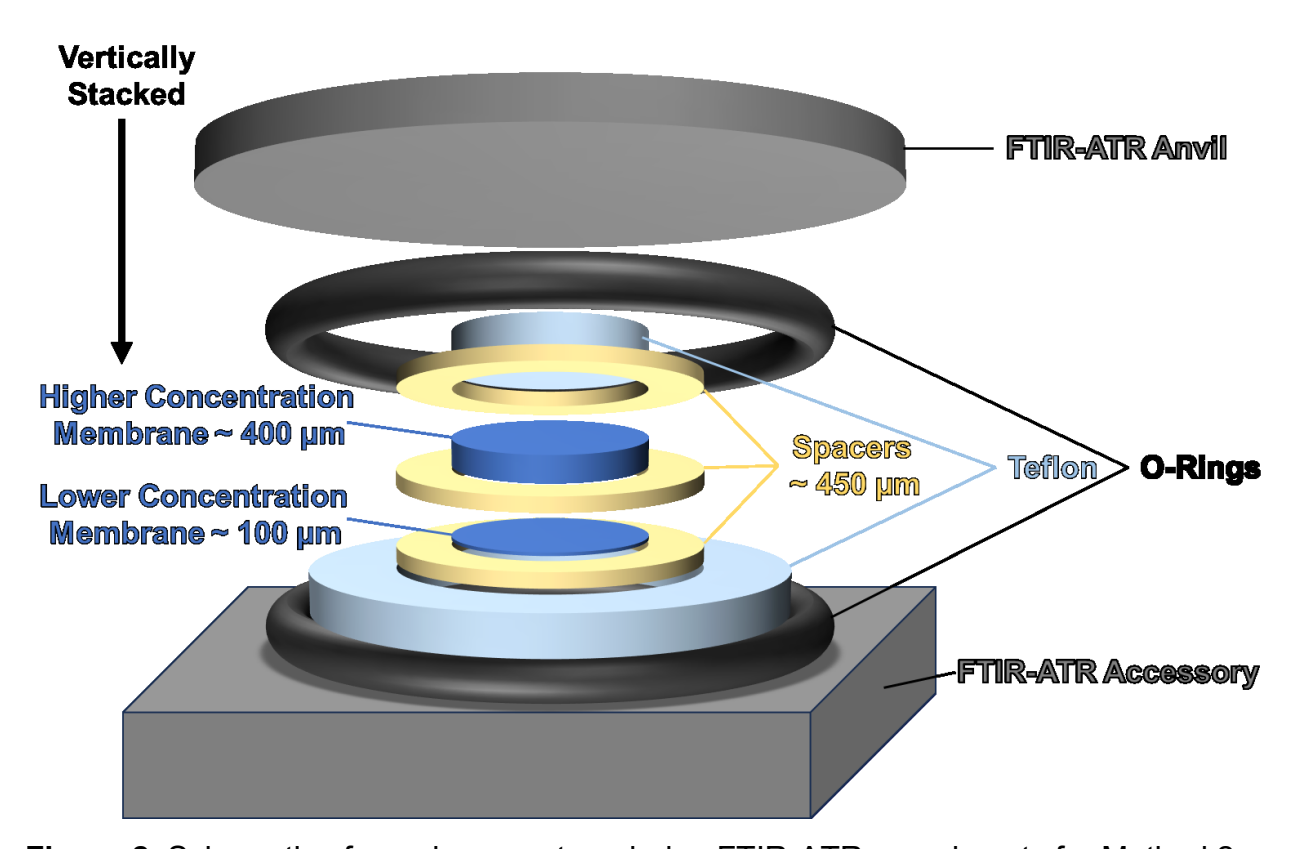


Figure 2. Schematic of membrane set up during FTIR-ATR experiments for Method 2.

The accessory was then removed from the glove box and returned to the FTIR. After thermal equilibration of the sample, the anvil was tightened further to induce contact between both membranes and spectral collection began in 10 s intervals for 320

min using the average of 4 scans. After data collection, the sample was removed, the ATR accessory was cleaned with isopropyl alcohol, and a background was collected. Note that only one diffusion measurement per sample is possible with this method.

One measurement and one replicate each at 5 different temperatures: 80, 90, 100, 110, and 120 °C were collected. At each temperature, 3 combinations of LiTFSI concentration were tested. The concentration pairs are reported in Table 2. The concentration difference was fixed at $\Delta r = 0.05 \, \mathrm{mol_{LiTFSI}/mol_{EO}}$. Although the concentration dependence of salt diffusion in PEO has been found to be weak, it is desirable to use a small concentration difference in order to minimize error from this effect. On the other hand, a large difference is desirable to maximize changes in the FTIR signal. Our prior work found that a difference of $0.05 \, \mathrm{mol_{LiTFSI}/mol_{EO}}$ is an acceptable compromise.²⁹

Table 2. Concentration pairs used for concentration-based diffusion measurements.

$r_{Bottom} (\text{mol}_{\text{LiTFSI}}/\text{mol}_{\text{EO}})$	$r_{Top} (\text{mol}_{\text{LiTFSI}}/\text{mol}_{\text{EO}})$
0.00	0.05
0.05	0.10
0.10	0.15

For the purposes of FTIR-ATR analysis, concentration in molarity (mol/L) can be analytically determined from r as follows:

$$c_{LiTFSI} = \left(\frac{r}{r * M_{LiTFSI} * V_{LiTFSI} + 1 * M_{EO} * V_{EO}}\right) \tag{4}$$

where M_i is molar mass and V_i is specific volume. EO represents a monomer repeat unit of PEO. Values are $M_{EO}=44.05\,\mathrm{g/mol}$, $M_{LiTFSI}=287.1\,\mathrm{g/mol}$, $V_{EO}=8\times10^{-7}T^2+5\times10^{-4}T+0.8756\,\mathrm{mL/g}$, and $V_{LiTFSI}=0.44\,\mathrm{mL/g}$. Specific volume for EO is taken from a quadratic fit to data from Zoller and Walsh for $5\times10^5\,\mathrm{g/mol}$ PEO in the amorphous state with T = $70-200\,\mathrm{^{\circ}C}$. Equation 4 assumes volume additivity. At $70\,\mathrm{^{\circ}C}$, concentration is $1.1\,\mathrm{mol/L}$ at $r=0.05\,\mathrm{mol_{LiTFSI}/mol_{EO}}$ and $2.5\,\mathrm{mol/L}$ at $r=0.15\,\mathrm{mol_{LiTFSI}/mol_{EO}}$.

Results and Discussion.

Thermal Gradient Induced Diffusion.

The FTIR-ATR spectra of the CF₃ stretching peak is shown in Figure 3. There are two parts to the experiment. The first part shown in Figure 3(a) entails applying a temperature gradient across the thickness of the polymer electrolyte membrane. Before the experiment begins, the sample is at 70°C, i.e. both ATR crystal and anvil are at 70°C. In this example, the ATR crystal is heated to 77.5°C and the anvil is cooled to 62.5°C. Time zero is taken as the point at which the temperature set points are reached. In Figure 3(a), the FTIR-ATR spectra are collected at 77.5°C and the initial spectra are red. With time the salt diffuses toward the cold side, due to thermal diffusion, and the peak intensity decreases until the final blue spectra, which occur at steady state when thermal diffusion is balanced by Fickian diffusion. After reaching steady state, the second part of the experiment is conducted and the system is returned to isothermal. This data, collected at the ATR crystal which is now held at 70°C, is shown in Figure 3(b). Over time the peak intensity increases as the thermal-gradient induced concentration gradient dissipates due to Fickian diffusion. Thus, Figure 3(b) is an example of a diffusion experiment going from a gradient of 62.5 °C / 77.5 °C to isothermal state: 70 °C / 70 °C. Due to the fact that thermal diffusion (of heat) is much faster than mass diffusion in polymer electrolytes, the temperature gradient dissipates much faster than the concentration gradient. In fact, great care was taken to define time zero as the point at which the boundary temperatures reached the set points. Therefore, it is assumed that the temperature gradient is negligible during the Fickian diffusion experiment. This means that the temperature dependence of the Fickian diffusion coefficient can be ignored, although it is important for thermal diffusion (of mass). 19 It also means and that the absorbance change is due to the change in concentration and not due the effect of temperature. 35 The magnified views in the insets of Figure 3 focus on the maxima of the CF₃ peak of LiTFSI from 1215-1156 cm⁻¹ to more clearly show the change with time. In both panels, red is the initial spectrum and blue is the spectrum at final time.

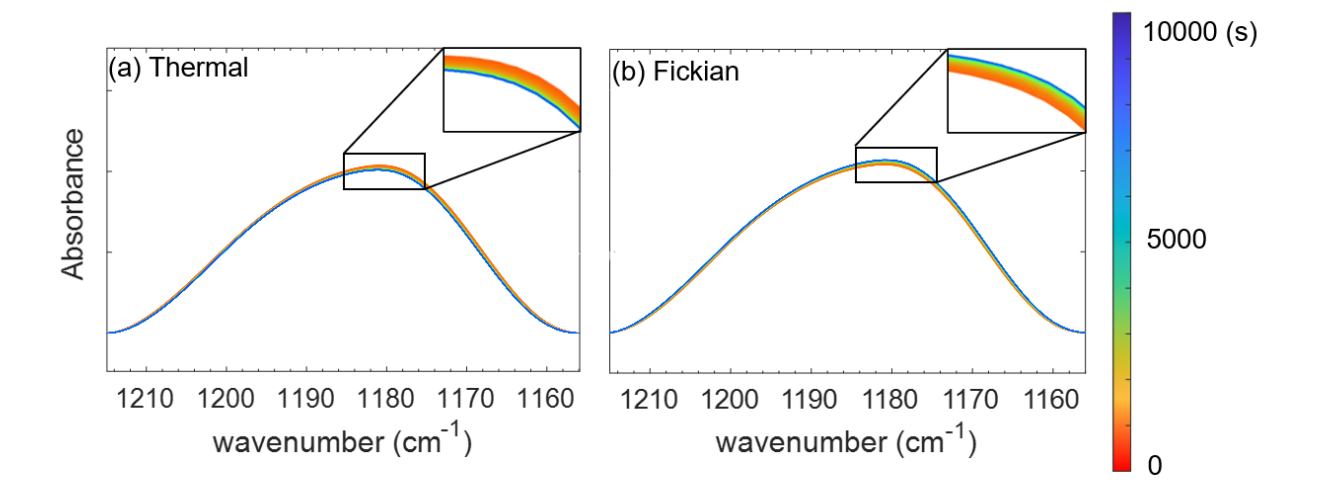


Figure 3. FTIR-ATR spectra of the CF_3 stretching peak, wavenumbers 1215-1156 cm⁻¹. **(a)** Thermal gradient FTIR-ATR experiment in which the peak begins with red when the sample is initially transitioned from the isothermal state at time zero to a temperature difference being applied $(70/70^{\circ}\text{C}\rightarrow62.5/77.5^{\circ}\text{C})$. The final spectra are blue when the system reaches a steady state due to thermal diffusion (driven by the temperature gradient) being balanced by Fickian diffusion. Thermal diffusion of the salt is from the hot ATR side, where measurement occurs, to the cold anvil. This causes the peak intensity to decrease from red to blue. **(b)** Isothermal FTIR-ATR measurement of Fickian diffusion in which the initial red peak occurs when the temperature difference is removed $(62.5/77.5^{\circ}\text{C} \rightarrow 70/70^{\circ}\text{C})$. During these isothermal measurements the concentration gradient that had been induced by thermal diffusion dissipates due to Fickian diffusion, which causes the peak intensity to increase with time from red to blue. The color map denotes the measurement times for both experiments.

In order to evaluate transport, i.e. transient changes, the integrated absorbance has been normalized from zero to one according to equation 1. This normalized absorbance is equal to normalized concentration because the constants of the Beer-Lambert law cancel. Therefore, diffusion models can be applied directly to normalized absorbance values without the need for calibration and without needing to know the absolute concentrations initially and at the boundaries of the membrane. The normalized absorbance from a characteristic measurement is shown in Figure 4 under the same conditions as Figure 3. In Figure 4(a), the thermal gradient causes the salt concentration to decrease at the ATR crystal, and the normalized absorbance is shown going down to emphasize this point. In Figure 4(b), the return to isothermal conditions

 $(62.5^{\circ}\text{C}/77.5^{\circ}\text{C} \rightarrow 70^{\circ}\text{C}/70^{\circ}\text{C})$ causes the concentration at the ATR crystal to increase, and the normalized absorbance is shown increasing. A numerical diffusion model was regressed to this data to determine the diffusion coefficient, and the best fit yields $D_{LiTFSI} = 3.996 \times 10^{-8} \, \text{cm}^2/\text{s}$. Analysis of thermal diffusion data requires development of a model, which is beyond the scope of this report. Therefore, only Fickian diffusion coefficients are reported in this work.

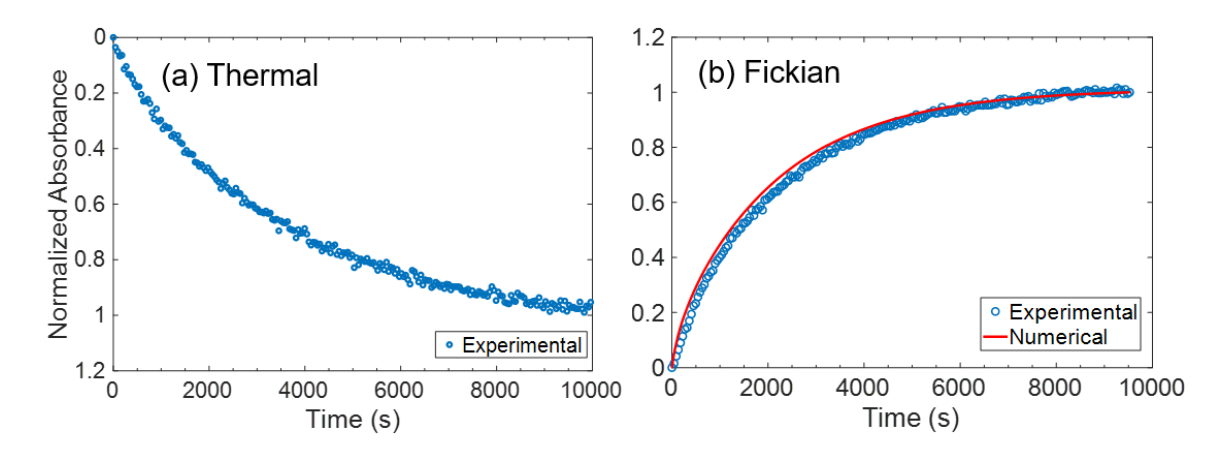


Figure 4. Normalized and integrated absorbance of the CF_3 peak gathered from FTIR-ATR temperature-based diffusion experiment. **(a)** Shows thermal diffusion $(70/70^{\circ}\text{C} \rightarrow 62.5/77.5^{\circ}\text{C})$, with normalized absorbance shown going down to emphasize the decrease in salt concentration at the ATR crystal due to the salt moving to the cold side during thermal diffusion. **(b)** Shows Fickian diffusion $(62.5/77.5^{\circ}\text{C} \rightarrow 70/70^{\circ}\text{C})$ with increasing normalized absorbance reflecting the increasing salt concentration at the ATR crystal as the concentration gradient is dissipated. The red curve is the best fit of a numerical diffusion model.

Diffusion coefficients were found by fitting a numerical solution of equation (2) to the normalized, integrated absorbance data in MATLAB as reported in Kim et al.²⁹ It can be seen from Figure 4(b) that the numerical model is a reasonably good fit to the experimental data. The diffusion coefficient value found from regression to the numerical model was used in an analytical model, and the result is shown in Figure S1. It is also a decent fit to the experimental data. In both models, concentration at the ATR crystal is a function of time, and diffusion coefficient and sample thickness are assumed constant. The change in FTIR-ATR signal was not sufficiently large to yield reproducible results with the 10 °C temperature difference. Diffusion coefficients from experiments returning to isothermal from 15 and 20 °C temperature differences are reported in

Tables S1 and S2 and compared to those from the concentration-based approach below.

Comparison to Concentration Based Diffusion.

Transient Fickian diffusion was also driven by a concentration gradient. As the experiments were conducted on solid polymer electrolytes, convection is not considered. No flux boundary conditions remain in this experiment, but the initial concentration profile is a step change rather than a linear profile. We have previously reported analytical and numerical solutions to this case. ^{27, 29} The specific thicknesses of the membranes in each experiment were used in the analysis. Results from the concentration-based diffusion measurements are shown in Table S3. In agreement with other reports of LiTFSI diffusion in PEO-based polymers, a non-monotonic concentration dependence is observed that is of questionable statistical significance. ^{29, 36} The root of this interesting behavior is not well understood, but is thought to be related to the complex polar and electrostatic interactions in the system resulting in a distribution of ion cluster sizes that depend on concentration and a population of lithium ions rather strongly coordinated to ether oxygens of PEO.

Results from both temperature-gradient and concentration-gradient based measurements are compared in Figure 5. Concentration-based measurements are shown for average molar ratios of $r_{avg}=0.075~{\rm and}~0.125~{\rm mol_{LiTFSI}/mol_{EO}}$. In other words, the two membrane concentrations were either $r=0.05~{\rm and}~0.10$ or $r=0.10~{\rm and}~0.15~{\rm mol_{LiTFSI}/mol_{EO}}$. The thermal-gradient experiments are reported at an isothermal temperature of 70 °C, which was chosen to ensure that the PEO phase was completely amorphous without encroaching on the upper temperature limit of the water bath. In order to maintain all parts of the sample above the crystallization temperature of PEO (55 °C) and the water bath sufficiently below the boiling point of water, while also applying large enough temperature difference for reproducible results, it was not possible to examine any isothermal temperature other than 70 °C in the thermal-gradient experiments. Higher temperatures are possible but would require a change to the experimental set-up. The concentration-based results were measured between 80 and 120 °C. Only shown are those results whose diffusion coefficient values are

statistically different from zero (based on one standard deviation). Also shown in Figure 5 are several literature reports of LiTFSI diffusion in SEO diblock copolymers at different temperatures and from different experimental methods. The salt concentration(s) from each study are reported in the legend and the molecular weight of the SEO is reported in the caption. As shown, each result from literature was reported at a single temperature only. Kim et al. is our prior work with concentration-gradient FTIR-ATR of LiTFSI diffusion in the SEO at 120 °C.²⁹ Timachova et al. reported the mutual diffusion coefficients of LiTFSI in SEO (32 kg/mol) at concentrations ranging from r = 0.06 to 0.30 mol $_{\rm LiTFSI}/{\rm mol}_{\rm EO}$, at 90 °C.³⁷ Finally, Mullin et al. reported LiTFSI mutual diffusion of LiTFSI in SEO (172 kg/mol) at $r_{avg} = 0.085$ and 90 °C. Both Timachova et al. and Mullin et al. used the electrochemical restricted diffusion method, in which a concentration gradient is induced by applying a constant current. Dissipation of the concentration gradient occurs when the current is removed. This is tracked via the cell potential, which is a less direct measurement of concentration, but one that can be calibrated to the concentration difference between the reversible electrodes.

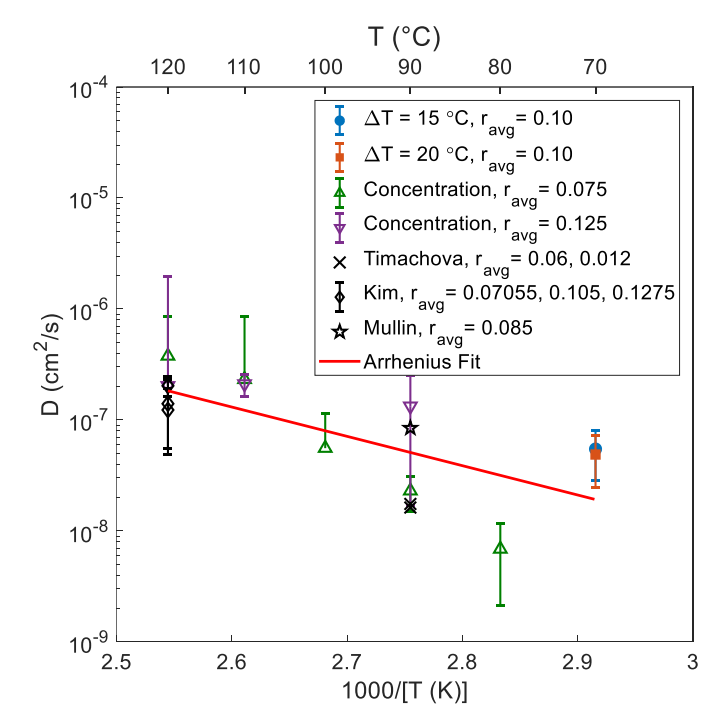


Figure 5. Diffusion coefficients of LiTFSI in SEO from the thermal gradient technique is shown as closed symbols. Fickian diffusion coefficients from the concentration gradient approach are shown as open symbols. Literature data is shown in black. The average molar ratios, r_{avq} , shown in the legend have units of $\text{mol}_{\text{LiTFSI}}/\text{mol}_{\text{EO}}$. The temperature

gradient used to induce a concentration gradient in the thermal gradient experiments is noted in the legend. The molar ratio difference between the 2 membranes used in the concentration-based experiments is 0.05 $\rm mol_{LiTFSI}/mol_{EO}$. Reports from literature for concentration-based FTIR-ATR: Kim et al. [SEO(121-165)/LiTFSI, $M_n = 286 \rm \, kg/mol$, $r_{avg} = 0.0775, 0.105, \rm and 0.1275 \, mol_{LiTFSI}/mol_{EO}, \ T = 120 \, ^{\circ}C],^{2}$ and for restricted diffusion: Timachova et al. [SEO(16-16)/LiTFSI, $M_n = 32 \rm \, kg/mol, \ r_{avg} = 0.06 \, and 0.12 \, mol_{LiTFSI}/mol_{EO}, \ T = 90 \, ^{\circ}C]^{37}$ and Mullin et al. [SEO(74-98)/LiTFSI, $M_n = 172 \rm \, kg/mol, \ r_{avg} = 0.085 \, mol_{LiTFSI}/mol_{EO}, \ T = 90 \, ^{\circ}C]$. Numbers in parentheses denote M_n of PS and PEO blocks, respectively, in kg/mol. Error bars represent one standard deviation.

There is a considerable amount of uncertainty in the reported diffusion coefficients, both within a study based on error bars and to a lesser extent between studies. All studies more or less agree within the certainty of one standard deviation, as is apparent from the overlapping error bars at each temperature. Variability is to be expected to some extent for a stochastic process such as diffusion. In the particular case of our concentration-gradient experiments, the procedure is quite challenging. The various o-rings and spacers along with the two small samples (shown in the experimental section) must all be carefully centered while working in a glove box (with bulky gloves). Moreover, repeat measurements require repeating this challenging procedure for every measurement, which results in rather poor reproducibility reflected in the large error bars seen in Figure 5. Comparing among different types of experiments (including literature), the cause of variation may be due to molar mass variation in the different block copolymers, as well as molecular structure. In the high molecular weight limit, segmental dynamics, which is not a function of molecular weight, is expected to correlate with salt mobility, but at lower molecular weight (such as that of Timachova et al.) chain-end effects can be significant. Correlation with segmental PEO dynamics has clearly been demonstrated for ionic conductivity that is driven by an electric potential gradient rather than a concentration gradient. Conductivity is fundamentally connected to the same ion mobilities that play a major role in determining salt diffusion.³⁸⁻⁴⁰ The variability between studies is not due in large part to differences in salt concentration, as various reports have shown that mutual diffusion of LiTFSI in PEO-based polymers is not a strong function of concentration.^{29, 36, 41-43} As shown in Figure 5 at 120 °C, the mutual diffusion coefficient of LiTFSI in SEO is between 10⁻⁶

and $10^{-7} \, \mathrm{cm^2/s}$. It drops a little less than an order of magnitude at 90 °C to between 2×10^{-8} to $2 \times 10^{-7} \, \mathrm{cm^2/s}$. For the most part, the collective reports of ion transport in literature follow an Arrhenius temperature dependence above 50 °C, the approximate crystallization temperature of PEO. Not only is this true for PEO-based polymers with LiTFSI, in which the electrolyte glass transition temperature, T_g , remains well below room temperature at all salt concentrations that are fully soluble, but also Arrhenius dependence is observed for conductivity of some other lithium salts in PEO electrolytes and for self-diffusion above 50 °C even if they exhibit some Vogel-Fulcher-Tammann (VFT) type curvature in the temperature dependence of ionic conductivity due to proximity to T_g .⁴⁴⁻⁴⁸ This Arrhenius dependence is to be expected for mutual diffusion in a condensed phase.¹⁹ In other words, diffusion coefficients increase with temperature because diffusion of ions and molecules in condensed media (liquids and solids) increases with increasing thermal energy that provides more frequent and larger fluctuations of random movements.⁴⁹ The Arrhenius equation for the pseudo-binary mutual diffusion coefficients reported here is

$$D = D_0 e^{\frac{E_a}{RT}}$$

where T is temperature (K), D is the diffusion coefficient (cm²/s), D_0 is a material constant (cm²/s), E_a is activation energy (J/mol), and R is the gas constant 8.314 [J/(mol K)]. The activation energy for an Arrhenius fit to all the data is $E_A = 50 \, \mathrm{kJ/mol}$ and the prefactor is $D_0 = 0.97 \, \mathrm{cm}^2/\mathrm{s}$. We are not aware of any reported values of activation energy for lithium salt mutual diffusion in PEO-based electrolytes. However, due to similarities observed between conductivity and diffusion in rubbery polymer electrolytes, we can compare activation energies reported for ionic conductivity in PEO-based electrolytes. These range from a little less than 10 to a little more than 100 kg/mol (i.e. about 0.1 to 1 eV), depending on the anion and the polymer architecture. $^{50-54}$ Both FTIR-ATR methods produce repeatable results, and, based on the reasonably good agreement among the various reports, we conclude that the FTIR-ATR methods are reasonably accurate. Moreover, this compilation of diffusion coefficients sets baseline values for future work on salt diffusion in polymer electrolytes to compare. The activation energy also makes it possible to estimate the magnitude of the diffusion coefficient on the hot side and cold side during the non-isothermal part of a thermal-

gradient experiment. For a 20 °C difference at an average temperature of 70 °C, the difference between the hot side $[D(80\,^{\circ}C)=3.9\times10^{-8}\,\mathrm{cm^2/s}]$ and cold side $[D(60\,^{\circ}C)=1.4\times10^{-8}\,\mathrm{cm^2/s}]$ is similar to the value at the average temperature $[D(70\,^{\circ}C)=2.4\times10^{-8}\,\mathrm{cm^2/s}]$. Thus, the exponential temperature dependence of diffusion makes modeling of the non-isothermal part of thermal-gradient experiments challenging. This challenge will be addressed in our future work in order to extract the thermal mass diffusion coefficient and thereby the Soret coefficient.

Concentration-gradient FTIR-ATR spectroscopy has disadvantages in comparison to the thermal-gradient FTIR-ATR method. First, an average, instead of exact concentration is used, as this method requires two samples to be stacked on top of each other in a complex set up done in the glove box. Between each measurement, the ATR assembly had to be moved back to the glovebox and new samples used for each replicate. The process of taking the FTIR-ATR in and out of the glovebox, as well as being unable to re-use samples, adds a significant amount of time to the set up and ease of the experimental process. This longer time also makes it more likely for errors to occur during each set up. With temperature-gradient induced diffusion, it is possible to re-use a sample, at a specific gradient, and test it as many times as needed. Additionally, all background scans can be run before (or after) the experiment for all temperatures tested, so that further glovebox work is not necessary.

Conclusions

Fickian diffusion coefficients were collected using two different experimental methods. One method used a temperature gradient to drive thermal diffusion and set-up a concentration gradient. Then, the temperature gradient was removed and the return to homogeneous salt distribution tracked to determine the diffusion coefficient. The second method used two membranes, each with different salt concentration, to induce diffusion. In both cases, time resolved FTIR-ATR spectroscopy was used to collect the data from which diffusion coefficients were determined.

FTIR-ATR is proven as an effective and repeatable means of measuring diffusion coefficients in solid systems, such as SEO/LiTFSI. With the comparison of previous literature all measurements agreed within experimental error. Understanding the

transport parameters surrounding Fickian diffusion in solid polymer electrolytes will aid in the development of optimal charge/discharge rates of batteries with non-ideal electrolytes.²⁹ Additionally, this project will serve as a standard of comparison for future measurements of mutual diffusion coefficients in polymer electrolytes and activation energy, which was found to be 50 kJ/mol. Characterizing the diffusion in polymer electrolytes has the potential to reduce the amount of heat waste being lost from heat production systems through utilization of thermogalvanic cells, which use a modest temperature gradient to create electricity. ³¹ However, further insight is needed on the effects that molecular structure, morphology, and molar mass have on the diffusion coefficients. Better understanding transport properties in solid polymer electrolytes would be significant for energy efficiency and battery technology.

Supporting Information

Temperature calibration description. Analytical model derivation and result. Tables of diffusion coefficient values.

Acknowledgments

The authors acknowledge funding from the Florida State University Council on Research and Creativity as well as the National Science Foundation award #1751450. We are indebted to Jeremy Phillips, Justin Pogge, Wade Robinson, and Tom Slade for their extensive help in designing, revising, and of course machining custom parts for our FTIR-ATR experiments. Without their continued assistance this work would not have been possible.

References

- 1. Pesko, D. M.; Timachova, K.; Bhattacharya, R.; Smith, M. C.; Villaluenga, I.; Newman, J.; Balsara, N. P., Negative transference numbers in poly (ethylene oxide)-based electrolytes. *Journal of The Electrochemical Society* **2017**, *164* (11), E3569-E3575, DOI:
- 2. Kim, K.; Kuhn, L.; Alabugin, I. V.; Hallinan, D. T., Lithium Salt Dissociation in Diblock Copolymer Electrolyte Using Fourier Transform Infrared Spectroscopy. *Frontiers in Energy Research* **2020**, *8* (240), DOI: 10.3389/fenrg.2020.569442.
- 3. Zhang, D.; Li, L.; Wu, X.; Wang, J.; Li, Q.; Pan, K.; He, J., Research Progress and Application of PEO-Based Solid State Polymer Composite Electrolytes. *Frontiers in Energy Research* **2021**, *9*, DOI: 10.3389/fenrg.2021.726738.

- 4. Wu, F.; Maier, J.; Yu, Y., Guidelines and trends for next-generation rechargeable lithium and lithium-ion batteries. *Chemical Society Reviews* **2020**, *49* (5), 1569-1614, DOI: 10.1039/c7cs00863e.
- 5. Tarascon, J. M.; Armand, M., Issues and challenges facing rechargeable lithium batteries. *Nature* **2001**, *414* (6861), 359-367, DOI: 10.1038/35104644.
- 6. Mullin, S. A.; Stone, G. M.; Panday, A.; Balsara, N. P., Salt Diffusion Coefficients in Block Copolymer Electrolytes. *Journal of The Electrochemical Society* **2011**, *158* (6), A619, DOI: 10.1149/1.3563802.
- 7. Zhang, H.; Liu, C.; Zheng, L.; Xu, F.; Feng, W.; Li, H.; Huang, X.; Armand, M.; Nie, J.; Zhou, Z., Lithium bis(fluorosulfonyl)imide/poly(ethylene oxide) polymer electrolyte. *Electrochimica Acta* **2014**, *133*, 529-538, DOI: https://doi.org/10.1016/j.electacta.2014.04.099.
- 8. Homann, G.; Stolz, L.; Nair, J.; Laskovic, I. C.; Winter, M.; Kasnatscheew, J., Poly(Ethylene Oxide)-based Electrolyte for Solid-State-Lithium-Batteries with High Voltage Positive Electrodes: Evaluating the Role of Electrolyte Oxidation in Rapid Cell Failure. *Scientific Reports* **2020**, *10* (1), 4390, DOI: 10.1038/s41598-020-61373-9.
- 9. Fenton, D. E.; Parker, J. M.; Wright, P. V., Complexes of alkali metal ions with poly(ethylene oxide). *Polymer* **1973**, *14* (11), 589, DOI: https://doi.org/10.1016/0032-3861(73)90146-8.
- 10. Singh, M.; Odusanya, O.; Wilmes, G. M.; Eitouni, H. B.; Gomez, E. D.; Patel, A. J.; Chen, V. L.; Park, M. J.; Fragouli, P.; latrou, H.; Hadjichristidis, N.; Cookson, D.; Balsara, N. P., Effect of molecular weight on the mechanical and electrical properties of block copolymer electrolytes. *Macromolecules* **2007**, *40* (13), 4578-4585, DOI: 10.1021/ma0629541.
- 11. Ferry, A.; Doeff, M. M.; DeJonghe, L. C., Transport property measurements of polymer electrolytes. *Electrochimica Acta* **1998,** *43* (10), 1387-1393, DOI: https://doi.org/10.1016/S0013-4686(97)10069-X.
- 12. Panday, A.; Mullin, S. A.; Gomez, E. D.; Wanakule, N. S.; Chen, V. L.; Hexemer, A.; Pople, J. A.; Balsara, N. P., Effect of Molecular Weight and Salt Concentration on Conductivity of Block Copolymer Electrolytes. *Macromolecules* **2009**, *42*, 4632-4637, DOI:
- 13. Hallinan, D. T.; Balsara, N. P., Polymer Electrolytes. *Annual Review of Materials Research* **2013**, 43 (1), 503-525, DOI: doi:10.1146/annurev-matsci-071312-121705.
- 14. Kim, K. Dissociation and Transport of Lithium lons in Polymer Electrolytes. Florida State University, Tallahassee, FL, 2021.
- 15. Ma, Y.; Doyle, M.; Fuller, T. F.; Doeff, M. M.; De Jonghe, L. C.; Newman, J., The Measurement of a Complete Set of Transport Properties for a Concentrated Solid Polymer Electrolyte Solution. *Journal of The Electrochemical Society* **1995**, *142* (6), 1859, DOI: 10.1149/1.2044206.
- 16. Kanematsu, T.; Sato, T.; Imai, Y.; Ute, K.; Kitayama, T., Mutual- and Self-Diffusion Coefficients of a Semiflexible Polymer in Solution. *Polymer Journal* **2005**, *37* (2), 65-73, DOI: 10.1295/polymj.37.65.
- 17. Herriot, C.; Khatun, S.; Fox, E. T.; Judeinstein, P.; Armand, M.; Henderson, W. A.; Greenbaum, S., Diffusion Coefficients from (13)C PGSE NMR Measurements-Fluorine-Free Ionic Liquids with the DCTA(-) Anion. *Journal of Physical Chemistry Letters* **2012**, *3* (3), 441-4, DOI: 10.1021/jz201700n.
- 18. Arnaud, R.; Benrabah, D.; Sanchez, J. Y., Theoretical Study of CF3SO3Li, (CF3SO2)2NLi, and (CF3SO2)2CHLi Ion Pairs. *The Journal of Physical Chemistry* **1996,** *100* (26), 10882-10891, DOI: 10.1021/jp953259q.
- 19. Silverman, M.; Hallinan, D., The relationship between self-diffusion activation energy and Soret coefficient in binary liquid mixtures. *Chemical Engineering Science* **2021**, *240*, 116660, DOI: https://doi.org/10.1016/j.ces.2021.116660.
- 20. Han, K. S.; Bazak, J. D.; Chen, Y.; Graham, T. R.; Washton, N. M.; Hu, J. Z.; Murugesan, V.; Mueller, K. T., Pulsed Field Gradient Nuclear Magnetic Resonance and Diffusion Analysis in Battery Research. *Chemistry of Materials* **2021**, *33* (22), 8562-8590, DOI: 10.1021/acs.chemmater.1c02891.

- 21. Ma, Y. P.; Doyle, M.; Fuller, T. F.; Doeff, M. M.; Dejonghe, L. C.; Newman, J., The Measurement of a Complete Set of Transport-Properties for a Concentrated Solid Polymer Electrolyte Solution. *Journal of the Electrochemical Society* **1995**, *142* (6), 1859-1868, DOI: 10.1149/1.2044206.
- 22. Pandey, A., Höfer, R., Taherzadeh, M., Nampoothiri, K. M., & Larroche, C., *Industrial Biorefineries and White Biotechnology*. Industrial Biorefineries and White Biotechnology, 2015, DOI: https://doi.org/10.1016/c2013-0-19082-4.
- 23. Silverstein, R. M.; Kiemle, D. J.; Webster, F. X., *Spectrometric identification of organic compounds*. 7th ed. / Robert M. Silverstein, Francis X. Webster, David J. Kiemle. ed.; John Wiley & Sons: Hoboken, NJ, 2005, DOI:
- 24. Song, K., 4 Interphase characterization in rubber nanocomposites. In *Progress in Rubber Nanocomposites*, Thomas, S.; Maria, H. J., Eds. Woodhead Publishing: 2017; pp 115-152, DOI: https://doi.org/10.1016/B978-0-08-100409-8.00004-8.
- 25. Levi, K.; Kwan, A.; Rhines, A. S.; Gorcea, M.; Moore, D. J.; Dauskardt, R. H., Emollient molecule effects on the drying stresses in human stratum corneum. *Br J Dermatol* **2010**, *163* (4), 695-703, DOI: 10.1111/j.1365-2133.2010.09937.x.
- 26. Elabd, Y. A.; Baschetti, M. G.; Barbari, T. A., Time-resolved Fourier transform infrared/attenuated total reflection spectroscopy for the measurement of molecular diffusion in polymers. *Journal of Polymer Science Part B: Polymer Physics* **2003**, *41* (22), 2794-2807, DOI:
- 27. Hallinan Jr., D. T., Attenuated Total Reflectance Mode for Transport through Membranes. In *Infrared Spectroscopy Perspectives and Applications*, El-Azazy, A. P. M.; Al-Saad, K.; El-Shafie, A. S., Eds. IntechOpen: London, 2022; p Online, DOI: 10.5772/intechopen.107869.
- 28. Wu, I. D.; Chang, F.-C., Determination of the interaction within polyester-based solid polymer electrolyte using FTIR spectroscopy. *Polymer* **2007**, *48* (4), 989-996, DOI: https://doi.org/10.1016/j.polymer.2006.12.045.
- 29. Kim, K.; Hallinan, D. T., Lithium Salt Diffusion in Diblock Copolymer Electrolyte Using Fourier Transform Infrared Spectroscopy. *The Journal of Physical Chemistry B* **2020**, *124* (10), 2040-2047, DOI: 10.1021/acs.jpcb.9b11446.
- 30. Köhler, W.; Morozov, K. I., The Soret Effect in Liquid Mixtures A Review. *Journal of Non-Equilibrium Thermodynamics* **2016**, *41* (3), 151, DOI: https://doi.org/10.1515/jnet-2016-0024.
- 31. Mentor, J. J.; Torres, R.; Hallinan, D. T., The Soret effect in dry polymer electrolyte. *Molecular Systems Design & Engineering* **2020**, *5* (4), 856-863, DOI: 10.1039/C9ME00145J.
- 32. Hallinan, D. T.; Rausch, A.; McGill, B., An electrochemical approach to measuring oxidative stability of solid polymer electrolytes for lithium batteries. *Chemical Engineering Science* **2016**, *154*, 34-41, DOI: https://doi.org/10.1016/j.ces.2016.06.054.
- 33. Hallinan, D. T. Transport in polymer electrolyte membranes using time-resolved FTIR-ATR spectroscopy. Drexel University, Philadelphia PA, 2009.
- 34. Zoller, P.; Walsh, D. J., *Standard pressure-volume-temperature data for polymers*. Technomic Pub. Co.: Lancaster, PA, 1995; p 412, DOI:
- 35. Yamashita, H.; Kakuta, N.; Kawashima, D.; Yamada, Y., Measurement of temperature-dependent diffusion coefficients of aqueous solutions by near-infrared simultaneous imaging of temperature and concentration. *Biomedical Physics & Engineering Express* **2018**, *4* (3), 035030, DOI: 10.1088/2057-1976/aab645.
- 36. Gao, K. W.; Balsara, N. P., Electrochemical properties of poly(ethylene oxide) electrolytes above the entanglement threshold. *Solid State Ionics* **2021**, *364*, 115609, DOI: https://doi.org/10.1016/j.ssi.2021.115609.
- 37. Timachova, K.; Villaluenga, I.; Cirrincione, L.; Gobet, M.; Bhattacharya, R.; Jiang, X.; Newman, J.; Madsen, L. A.; Greenbaum, S. G.; Balsara, N. P., Anisotropic Ion Diffusion and Electrochemically

- Driven Transport in Nanostructured Block Copolymer Electrolytes. *The Journal of Physical Chemistry B* **2018,** *122* (4), 1537-1544, DOI: 10.1021/acs.jpcb.7b11371.
- 38. Fullerton-Shirey, S. K.; Maranas, J. K., Effect of LiClO4 on the Structure and Mobility of PEO-Based Solid Polymer Electrolytes. *Macromolecules* **2009**, *42* (6), 2142-2156, DOI: 10.1021/ma802502u.
- 39. Do, C.; Lunkenheimer, P.; Diddens, D.; Götz, M.; Weiß, M.; Loidl, A.; Sun, X.-G.; Allgaier, J.; Ohl, M., Li+ Transport in Poly(Ethylene Oxide) Based Electrolytes: Neutron Scattering, Dielectric Spectroscopy, and Molecular Dynamics Simulations. *Physical Review Letters* **2013**, *111* (1), 018301, DOI:
- 40. Borodin, O.; Smith, G. D., Mechanism of ion transport in amorphous poly(ethylene oxide)/LiTFSI from molecular dynamics simulations. *Macromolecules* **2006**, *39* (4), 1620-1629, DOI: 10.1021/ma052277v.
- 41. Hoffman, Z. J.; Shah, D. B.; Balsara, N. P., Temperature and concentration dependence of the ionic transport properties of poly(ethylene oxide) electrolytes. *Solid State Ionics* **2021**, *370*, 115751, DOI: https://doi.org/10.1016/j.ssi.2021.115751.
- 42. Galluzzo, M. D.; Loo, W. S.; Wang, A. A.; Walton, A.; Maslyn, J. A.; Balsara, N. P., Measurement of Three Transport Coefficients and the Thermodynamic Factor in Block Copolymer Electrolytes with Different Morphologies. *The Journal of Physical Chemistry B* **2020**, *124* (5), 921-935, DOI: 10.1021/acs.jpcb.9b11066.
- 43. Edman, L.; Ferry, A.; Oradd, G., Analysis of diffusion in a solid polymer electrolyte in the context of a phase-separated system. *Physical Review E* **2002**, *65* (4), DOI: 10.1103/PhysRevE.65.042803.
- 44. Volel, M.; Armand, M.; Gorecki, W., Influence of sample history on the morphology and transport properties of PEO-lithium salt complexes. *Macromolecules* **2004,** *37* (22), 8373-8380, DOI: 10.1021/ma0490404.
- 45. Gorecki, W.; Donoso, P.; Berthier, C.; Mali, M.; Roos, J.; Brinkmann, D.; Armand, M. B., NMR, DSC and conductivity study of the polymer solid electrolytes P(EO) (LiCp+1F2p+3SO3)x. *Solid State Ionics* **1988**, *28-30*, 1018-1022, DOI: https://doi.org/10.1016/0167-2738(88)90323-2.
- 46. Arumugam, S.; Shi, J.; Tunstall, D. P.; Vincent, C. A., Cation and anion diffusion coefficients in a solid polymer electrolyte measured by pulsed-field-gradient nuclear magnetic resonance. *Journal of Physics: Condensed Matter* **1993**, *5* (2), 153, DOI: 10.1088/0953-8984/5/2/003.
- 47. Zahurak, S.; Kaplan, M.; Rietman, E.; Murphy, D.; Cava, R., Phase relationships and conductivity of the polymer electrolytes poly (ethylene oxide)/lithium tetrafluoroborate and poly (ethylene oxide)/lithium trifluoromethanesulfonate. *Macromolecules* **1988**, *21* (3), 654-660, DOI:
- 48. Deng, C.; Webb, M. A.; Bennington, P.; Sharon, D.; Nealey, P. F.; Patel, S. N.; de Pablo, J. J., Role of Molecular Architecture on Ion Transport in Ethylene oxide-Based Polymer Electrolytes. *Macromolecules* **2021**, *54* (5), 2266-2276, DOI: 10.1021/acs.macromol.0c02424.
- 49. James Welty, C. E. W., Gregory L. Rorrer, *Fundamentals of Momentum, Heat, and Mass Transfer* 5th ed.; Wiley: 2007; p 728, DOI:
- 50. Chintapalli, M.; Le, T. N. P.; Venkatesan, N. R.; Mackay, N. G.; Rojas, A. A.; Thelen, J. L.; Chen, X. C.; Devaux, D.; Balsara, N. P., Structure and Ionic Conductivity of Polystyrene-block-poly(ethylene oxide) Electrolytes in the High Salt Concentration Limit. *Macromolecules* **2016**, *49* (5), 1770-1780, DOI: 10.1021/acs.macromol.5b02620.
- 51. Devaux, D.; Bouchet, R.; Gle, D.; Denoyel, R., Mechanism of ion transport in PEO/LiTFSI complexes: Effect of temperature, molecular weight and end groups. *Solid State Ionics* **2012**, *227*, 119-127, DOI: 10.1016/j.ssi.2012.09.020.
- 52. Gorecki, W.; Jeannin, M.; Belorizky, E.; Roux, C.; Armand, M., PHYSICAL-PROPERTIES OF SOLID POLYMER ELECTROLYTE PEO(LITFSI) COMPLEXES. *Journal of Physics-Condensed Matter* **1995**, *7* (34), 6823-6832, DOI: 10.1088/0953-8984/7/34/007.

- 53. Rietman, E. A.; Kaplan, M. L.; Cava, R. J., Lithium ion-poly (ethylene oxide) complexes. I. Effect of anion on conductivity. *Solid State Ionics* **1985**, *17* (1), 67-73, DOI: https://doi.org/10.1016/0167-2738(85)90124-9.
- 54. Ferloni, P.; Chiodelli, G.; Magistris, A.; Sanesi, M., Ion transport and thermal properties of poly(ethylene oxide) LiClO4 polymer electrolytes. *Solid State Ionics* **1986**, *18-19*, 265-270, DOI: https://doi.org/10.1016/0167-2738(86)90124-4.

TOC Graphic

